

A unified picture for the γ -ray and prompt optical emissions of GRB 990123

A. Panaitescu¹ & P. Kumar²

¹ *Space Science and Applications, Los Alamos National Laboratory, Los Alamos, NM 87545, USA*

² *Department of Astronomy, University of Texas, Austin, TX 78712*

ABSTRACT

The prompt optical emission of GRB 990123 was uncorrelated to the γ -ray light-curve and exhibited temporal properties similar to those of the steeply-decaying, early X-ray emission observed by Swift at the end of many bursts. These facts suggest that the optical counterpart of GRB 990123 was the large-angle emission released during (the second pulse of) the burst. If the optical and γ -ray emissions of GRB 990123 have, indeed, the same origin then their properties require that (i) the optical counterpart was synchrotron emission and γ -rays arose from inverse-Compton scatterings (the "synchrotron self-Compton model"), (ii) the peak-energy of the optical-synchrotron component was at ~ 20 eV, and (iii) the burst emission was produced by a relativistic outflow moving at Lorentz factor $\gtrsim 450$ and at a radius $\gtrsim 10^{15}$ cm, which is comparable to the outflow deceleration radius. Because the spectrum of GRB 990123 was optically thin above 2 keV, the magnetic field behind the shock must have decayed on a length-scale of $\lesssim 1\%$ of the thickness of the shocked gas, which corresponds to $10^6 - 10^7$ plasma skin-depths. Consistency of the optical counterpart decay rate and its spectral slope (or that of the burst, if they represent different spectral components) with the expectations for the large-angle burst emission represents the most direct test of the unifying picture proposed here for GRB 990123.

Key words: gamma-rays: bursts - radiation mechanisms: non-thermal - shock waves

1 INTRODUCTION

The Swift satellite has evidenced the existence (in a majority of bursts) of a fast-decaying phase after the end of γ -ray emission (e.g. O'Brien et al. 2006), during which the 0.3–10 keV flux falls-off as $F_x \propto t^{-(1.5-4)}$. The emission of the optical counterpart of GRB 990123, measured by ROTSE (Akerlof et al. 1999), has a similarly steep decay, $F_o \propto t^{-(1.5-2.5)}$ at about the same time (50–400 s after trigger) as the fast-decaying phase of Swift X-ray afterglows. This similarity suggests that the optical counterpart of GRB 990123 and the fast decay phase of Swift X-ray afterglows originate from the same shock of the GRB relativistic outflow. In Swift bursts, the transition from the prompt emission to the fast X-ray decay is continuous, which indicates that the γ -ray and X-ray emissions also have a common origin. This leads to the conjecture that the optical and γ -ray emissions of GRB 990123 arise from the same shock.

As shown in figure 2 of Galama et al. (1999), the prompt optical emission of GRB 990123 is well above the extrapolation of the burst continuum to lower energies. Then, if the optical and burst emission originate from the same part of the outflow, they must represent different spectral components, i.e. optical must be synchrotron emission and γ -ray must be inverse-Compton scatterings. This is the "synchrotron self-Compton model" which has been used by

Panaitescu & Mészáros (2000) and Stern & Poutanen (2004) to explain the hard low-energy spectra observed for some BATSE bursts (Preece et al. 1998). Kumar et al. (2006) have shown that the temporal and spectral properties of GRBs 050126 and 050219A favour this model for the γ -ray emission.

As discussed by Nousek et al. (2006) and Zhang et al. (2006), the fast-decay phase of Swift afterglows can be identified with the "large-angle emission" released during the burst, i.e. the emission from the fluid moving at an angle θ larger than the inverse of the outflow's Lorentz factor Γ , with θ measured relative to the outflow center – observer axis. Any radiating GRB outflow whose opening is larger than Γ^{-1} yields a large-angle emission, irrespective of the type of shock (internal, reverse-external, or forward-external) and radiative process. As shown by Kumar & Panaitescu (2000), relativistic effects lead to a simple relation between the spectral slope and decay index of the fast-decaying X-ray afterglow, which is generally found to be consistent with the observations.

If, as argued above, the prompt optical emission of GRB 990123 and the fast-decay phase of Swift X-ray afterglows have the same origin, then the former could also be identified with the large-angle emission produced during the burst. This conjecture can explain why the optical emission of GRB 990123 appears uncorrelated with that at γ -rays. As shown

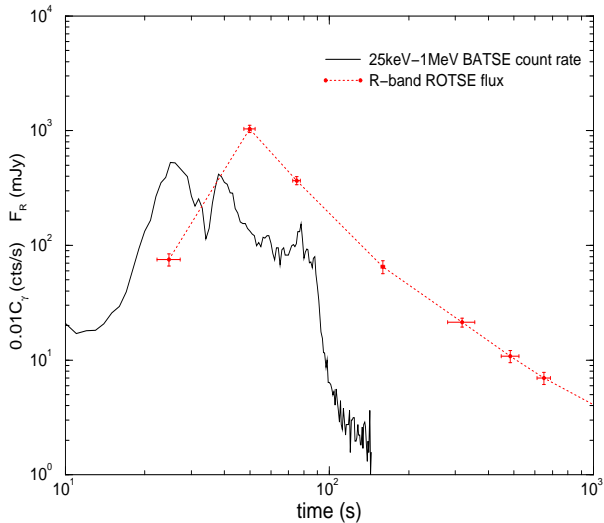


Figure 1. The BATSE 25–1000 keV count-rate for GRB 990123, with 1 s time resolution, and the ROTSE *R*-band light-curve of its optical counterpart.

in Figure 1, the optical emission of GRB 990123 is weaker during the first pulse, exhibits a maximum during the tail of the second pulse (which peaks at 38 s), and then decays monotonically throughout the third GRB pulse and after the burst end. The decoupling of the optical and γ -ray emissions of GRB 990123 can be explained if the optical counterpart is identified with the large-angle emission released during the second GRB pulse (when the optical counterpart peaks) and if the optical emission of other pulses is weaker than that of the second GRB pulse. Given the simple structure of GRB 990123 light-curve and the sparse sampling of the optical counterpart, the lack of an optical- γ -ray temporal correlation could also be the result of fluctuations in the optical-to- γ -ray output ratio from pulse to pulse. Thus, the large-angle emission is not a unique explanation for the uncorrelated optical and burst emissions of GRB 990123; it just represents a possible reason and a working assumption for the calculations below.

Based on the above arguments, in this work we attribute the optical prompt emission of GRB 990123 to the large-angle synchrotron emission produced during the second GRB pulse and identify the prompt γ -ray emission with up-scatterings of the synchrotron photons. The observational constraints imposed on this scenario are presented in §2 and used in §3 to determine the outflow parameters which accommodate them. In §4, we discuss some implications of the large-angle emission scenario for the optical counterpart and a possible shortcoming of the synchrotron self-Compton model, which can be circumvented if the magnetic field decays and does not fill the entire GRB outflow.

We emphasize two aspects of the following treatment of the unification of the γ -ray and prompt optical emissions of GRB 990123.

First, we do not assume a certain mechanism for the dissipation of the relativistic outflow energy. This mechanism could be (*i*) internal shocks in an unsteady wind, as proposed by Mészáros & Rees (1999), or (*ii*) the external reverse-shock, as proposed by Sari & Piran (1999) (fig. 1 of Panaitescu & Mészáros 1998 also shows that a 10–16th mag-

nitude optical emission could arise from the reverse-shock), and further investigated by Kobayashi & Sari (2000), Soderberg & Ramirez-Ruiz (2002), Fan et al. (2002), Panaitescu & Kumar (2004), Nakar & Piran (2005), and McMahon, Kumar & Piran (2006). Thus, the scenario proposed here does not represent a new theoretical framework for the GRB emission.

Second, the calculations below address primarily the implications of the proposed unifying scenario and represent a test of that scenario only to the extent that the resulting physical parameters are plausible. Otherwise, the proposed scenario for the optical counterpart of GRB 990123 is motivated by (*i*) the similarity between its temporal properties and those of the X-ray emission following Swift bursts, and (*ii*) the identification of the latter with the large-angle burst emission. The only observational test for the proposed scenario is the consistency between the decay of the optical emission of GRB 990123 and the expectation from the large-angle emission for the measured low-energy slope of the burst spectrum (§2).

2 OPTICAL AND GAMMA-RAY EMISSIONS OF GRB 990123

The optical measurements of GRB 990123, shown in figure 1, are too sparse to pinpoint when the flux peaked, but sufficient to show that a substantial fraction of the post-peak optical flux arose during the second GRB pulse. As burst emission episodes may be dynamically independent, the decay of the ROTSE optical emission should be timed from the onset of the second GRB pulse, which occurred at ~ 30 s after the GRB trigger, as shown in Figure 2. The optical counterpart emission decays as a power in time $F(t) \propto t^{-\alpha}$, with index $\alpha \simeq 1.5$.

The available optical coverage of Swift afterglows indicates that, quite often, the optical emission decays as a power-law from the first observations, at only 100–200 s after trigger (see figure 1 of Panaitescu et al. 2006). This suggests that the forward-shock contributes to the optical emission just at the end of the burst and motivates us to back-extrapolate the 0.1–2 day optical emission of GRB afterglow 990123 to the epoch of the ROTSE observations and subtract it to determine the optical emission at that time which is excess of the forward-shock contribution. As shown in Figure 2, the ROTSE excess emission has a decay index $\alpha = 1.8 \pm 0.1$, but the power-law fit is not that good, having $\chi^2 = 6.4$ for 4 degrees of freedom. The reason is that the excess emission exhibits a steepening decay, from $\alpha = 1.3 \pm 0.3$ for the first two measurements after the second GRB pulse to $\alpha = 2.0 \pm 0.2$ during the last four measurements (figure 2).

If the decay of the ROTSE optical flux is indeed the large-angle emission produced during the burst and if this emission switches-off sufficiently fast, then the slope β_o of the optical spectral energy distribution (SED), $F_\nu \propto \nu^{\beta_o}$, must be

$$\beta_o = 2 - \alpha \quad (1)$$

(Kumar & Panaitescu 2000). Thus, the above possible decay indices α of the ROTSE optical emission imply that $0 < \beta_o < 0.7$. The consistency of β_o with the burst SED

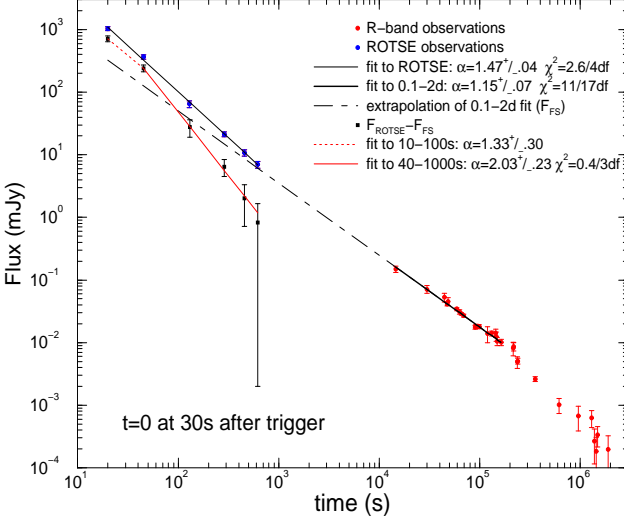


Figure 2. The 0.1–2 day optical light-curve of GRB 990123 (red symbols), fit with a power-law decay (thick, solid line), extrapolated to the epoch of ROTSE observations (blue symbols) and subtracted to isolate the early optical emission in excess of that from the forward-shock (black symbols). This excess emission exhibits an increasing decay rate after 50 s. Time is measured from 30 s after trigger, which is when the second GRB pulse starts (this pulse peaks about 8 s after its beginning and 12 s before the largest optical flux measured by ROTSE). The excess optical emission can arise in the same mechanism that generated the burst, its continuation after the end of the burst (which is at 60 s) being due to the large-angle prompt emission.

slope at low-energy (20–300 keV), which Briggs et al. (1999) report to be $\beta_{LE} = 0.4 \pm 0.1$, supports the synchrotron self-Compton interpretation for the optical and γ -ray emissions of GRB 990123 because, in this model, the SED of synchrotron and inverse-Compton components must have the same spectral slopes at frequencies above self-absorption. Therefore, the SED of the emission of GRB 990123’s optical counterpart should be

$$F_\epsilon \propto \begin{cases} \nu^{1/3} & \epsilon < \epsilon_{p,sy} \\ \nu^{-\beta_{HE}} & \epsilon > \epsilon_{p,sy} \end{cases} \quad (2)$$

as the only expected spectral slope consistent with β_o and β_{LE} is $1/3$.

$\beta_o = 1/3$ corresponds to the optical range being above the self-absorption energy, $\epsilon_{a,sy}$, but below the peak-energy of the synchrotron spectrum, $\epsilon_{p,sy}$. $\beta_{LE} = 1/3$ implies that the 20–300 keV range is between $\epsilon_{a,ic} = \gamma_p^2 \epsilon_{a,sy}$ and $\epsilon_{p,ic} = \gamma_p^2 \epsilon_{p,sy}$, where γ_p is the peak Lorentz factor of the electron distribution with energy in the shocked fluid and $\epsilon_{p,ic}$ is the peak-energy of the burst spectrum.

The low-energy spectrum of GRB 990123, $F_\nu \propto \nu^{-\beta_{LE}}$ peaks at an energy which is a fraction $\beta_{LE}/(\beta_{LE} + 1)$ of the peak-energy E_p of the νF_ν spectrum. According to Briggs et al. (1999), $E_p \simeq 720$ keV for the second GRB pulse, therefore

$$\epsilon_{p,ic}(t_p) = 210 \text{ keV} . \quad (3)$$

The burst SED at high-energy (1–10 MeV) is a power-law of slope $\beta_{HE} = -2.1 \pm 0.1$ (Briggs et al. 1999). This shows that the γ_p -electrons at the peak of the power-law electron distribution with energy,

$$\frac{dN}{d\gamma}(\gamma > \gamma_p) \propto \gamma^{-p} \quad (4)$$

do not cool radiatively because, in the opposite case, the distribution of cooled electrons, $dN/d\gamma \propto \gamma^{-2}$, would yield a much harder GRB spectrum ($F_\nu \propto \nu^{-1/2}$) above its peak energy. Barring a chance situation where γ_p is equal to the Lorentz factor γ_c above which all electrons undergo a significant radiatively cooling, this shows that $\gamma_c^2 \epsilon_{c,sy} > 10$ MeV, where $\epsilon_{c,sy}$ is the synchrotron energy at which the γ_c -electrons radiate. Then, $\epsilon_{p,ic} = \gamma_p^2 \epsilon_{p,sy} = 210$ keV, $\epsilon_{p,sy} \propto \gamma_p^2$, and $\epsilon_{c,sy} \propto \gamma_c^2$, lead to $\gamma_c/\gamma_p > (10^4/210)^{1/4}$:

$$\gamma_c \gtrsim 2.6 \gamma_p . \quad (5)$$

Furthermore, the observed high-energy burst spectral slope implies that the electron distribution index is $p = 2\beta_{HE} + 1 \simeq 5.2$.

The emission released at a radius r by some fluid patch moving at an angle θ relative to the direction toward the observer arrives at observer at time

$$ct = \frac{1}{2}r(\theta^2 + \Gamma^{-2}) \quad (6)$$

where Γ is the bulk Lorentz factor of the GRB-emitting source, and is Doppler-boosted by a factor

$$\mathcal{D} = \frac{2\Gamma}{\Gamma^2\theta^2 + 1} . \quad (7)$$

As discussed in §1, in the large-angle emission interpretation for the optical counterpart of GRB 990123, the optical emission is released during the second GRB pulse (which peaks at time $t_p = 8$ s after the beginning of the second GRB pulse). For a source whose emission switches-off instantaneously, the emission received at t_p comes from the fluid moving at angle $\theta = \Gamma^{-1}$ relative to the direction toward the observer. From equations (6) and (7), that emission arrives at $t_p = r/(c\Gamma^2)$ and is boosted by $\mathcal{D}(t_p) = \Gamma$. After t_p , emission arrives from $\theta > \Gamma^{-1}$, for which $t/t_p = (\Gamma^2\theta^2 + 1)/2$ and

$$\mathcal{D}(t) = \mathcal{D}(t_p) \frac{t_p}{t} \quad (8)$$

on virtue of equations (6) and (7).

Therefore, the large-angle emission arriving at fixed observer frequency corresponds to an ever-increasing comoving-frame frequency. Then, the above conclusion that, for GRB 990123, optical is below the peak-energy of the synchrotron spectrum ($\epsilon_{p,sy}$) implies that the synchrotron light-curve should steepen at t_+ when $\epsilon_{p,sy}$ crosses the optical domain:

$$2 \text{ eV} = \epsilon'_{p,sy} \mathcal{D}(t_+) = \epsilon'_{p,sy} \mathcal{D}(t_p) \frac{t_p}{t_+} = \epsilon_{p,sy} \frac{t_p}{t_+} \quad (9)$$

where prime denotes a quantity in the comoving-frame. The ROTSE emission with the forward-shock contribution subtracted (Figure 2) shows such a steepening at about 45 s, the subsequent decay index, $\alpha \simeq 2$, implying an optical SED slope $\beta_o \simeq 0$, as expected at the peak of synchrotron spectrum. For now, we parameterize the time when t_+ relative to the epoch of the second GRB pulse peak: $t_+ = x t_p$. Therefore, the observer-frame synchrotron peak-energy is

$$\epsilon_{p,sy}(t_p) = 2x \text{ eV} \quad x > 1 . \quad (10)$$

The extrapolation of the power-law fit to the ROTSE

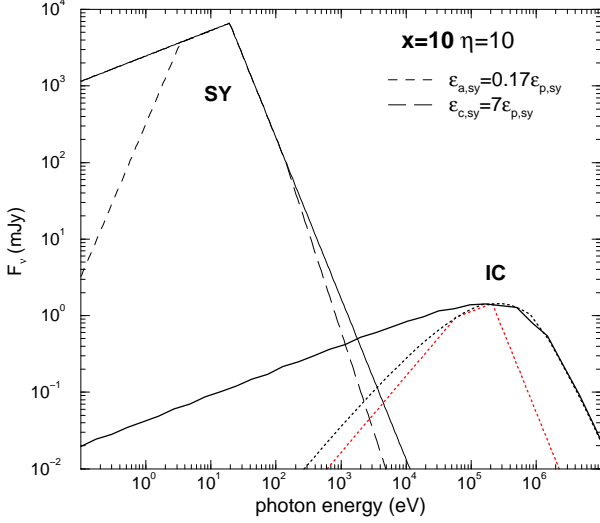


Figure 3. Synchrotron (optical) and inverse-Compton (γ -ray) components for GRB 990123. The synchrotron SED is the simplified spectrum given in equation (2) and has the peak frequency and flux given in equations (10) and (11) for $x = 10$. The inverse-Compton spectrum is calculated by integrating the scattered emissivity per electron over the electron distribution (equation 4). Dotted curves show the effect of self-absorption for $\epsilon_{a,sy} = 0.17\epsilon_{p,sy}$, (equation 49). Dashed line shows the effect of electron cooling for $\epsilon_{c,sy} = 7\epsilon_{p,sy}$ (equation 5). For comparison, the dot-dashed curve shows the inverse-Compton spectrum for monoenergetic electrons with γ_p given in equation (16).

light-curve to t_p , predicts an optical flux of $F_R(t_p) = 4$ Jy. The extrapolation of the forward-shock (FS) emission to the same time is $F_{FS}(t_p) = 0.93$ Jy, therefore the peak of the excess optical emission (which we attribute to the same mechanism as the burst itself) is $F_{sy}(t_p) = F_R(t_p) - F_{FS}(t_p) = 3.07$ Jy (the forward-shock emission may have started later than the optical peak time, in which case the $F_{sy}(t_p)$ above underestimates the true synchrotron flux by 25%). Taking into account that the slope of the optical SED is $\beta_o = 1/3$, it follows that the flux at the peak of the synchrotron spectrum is

$$F_{p,sy}(t_p) = F_{sy}(t_p) \left(\frac{\epsilon_{p,sy}}{2 \text{ eV}} \right)^{1/3} = 3.1 x^{1/3} \text{ Jy} . \quad (11)$$

The flux $F_{p,ic}$ at the peak-energy $\epsilon_{p,ic}$ keV of the inverse-Compton spectrum can be derived from the 100 keV flux of 0.61 mJy reported by Briggs et al. (1999) at 17 s after the onset of the second GRB pulse and from the burst flux decrease by about 40% from $t_p = 8$ s to 17 s:

$$F_{p,ic}(t_p) = (210/100)^{\beta_{LE}} \times 1.75 F_{100k}(17 \text{ s}) \simeq 1.5 \text{ mJy} . \quad (12)$$

Figure 3 shows schematically the synchrotron and inverse-Compton SED, the characteristics of the former having been derived above in the large-angle emission interpretation of the optical counterpart, while those of the latter come directly from observations.

Equations (3), (5), (10), (11) and (12) represent the conditions which we use to constrain the physical parameters of the synchrotron self-Compton model for the ROTSE optical and BATSE γ -ray emissions of GRB 990123. An upper limit on the parameter x is obtained if the synchrotron power-law spectrum above $\epsilon_{p,sy}$ extends up to the γ -ray range, i.e. there

are no other spectral breaks but $\epsilon_{c,sy}$, by requiring that the synchrotron flux at 2 keV (the lowest X-ray observational frequency) does not exceed the inverse-Compton flux:

$$F_{p,sy} \left(\frac{\epsilon_{i,sy}}{\epsilon_{c,sy}} \right)^{\beta_{HE}} \left(\frac{\epsilon_{c,sy}}{2 \text{ keV}} \right)^{\beta_{HE}+0.5} < F_{p,ic} \left(\frac{2 \text{ keV}}{\epsilon_{p,ic}} \right)^{\beta_{LE}} \quad (13)$$

which leads to $x < 14$ for $\epsilon_{c,sy} = 7\epsilon_{p,sy}$, which is the lowest value of the cooling energy (see equation 5), and to $x < 9$ for $\epsilon_{c,sy} > 2$ keV. Therefore, under the assumption that the synchrotron spectrum extends up keV energies, the peak-energy of the synchrotron spectrum should satisfy

$$x \lesssim 7 - 14 \quad (14)$$

and should cross the optical at $t_+ = x t_p < 115$ s after the peak of the second GRB pulse (145 s after trigger). If ROTSE emission is mostly the large-angle emission of the second GRB pulse then the optical light-curve should exhibit a break at t_+ , which is consistent with observations (see Figure 2). Based on the constraint above, we normalize x to 10.

3 SYNCHROTRON AND INVERSE-COMPTON EMISSIONS

Integrating the scattering photon spectrum per electron (e.g. equation 2.48 of Blumenthal & Gould 1970) over the synchrotron spectrum (equation 2) and over the electron distribution (equation 4), we obtain that

$$\epsilon_{p,ic} = 0.82 \gamma_p^2 \epsilon_{p,sy} . \quad (15)$$

Therefore, the typical electron Lorentz factor in the shocked fluid is

$$\gamma_p = \left(\frac{\epsilon_{p,ic}}{0.82 \epsilon_{p,sy}} \right)^{1/2} = 110 x_1^{-1/2} , \quad (16)$$

where $x_1 = x/10$ (the notation convention $Q_n = Q/10^n$ will be use hereafter).

The observed peak-energy of the synchrotron spectrum is

$$\epsilon_{p,sy} = \frac{4}{3} \Gamma \frac{\epsilon'_{p,sy}}{z+1} \quad (17)$$

where the factor 4/3 accounts for the flux-weighted average frequency (from equation 7, Doppler boost decreases from $\mathcal{D} = 2\Gamma$ at $\theta = 0$ to $\mathcal{D} = \Gamma$ at $\theta = \Gamma^{-1}$ and goes asymptotically to zero for $\theta \rightarrow \pi$), z is the burst redshift and

$$\epsilon'_{p,sy} = \frac{3\psi(p)}{4\pi} \frac{eh}{m_e c} \gamma_p^2 B \quad (18)$$

is the comoving-frame peak-energy of the synchrotron spectrum, B being the magnetic field in the shocked fluid and $\psi(p)$ a factor which a weak dependence on the electron index p . By integrating the synchrotron emissivity per electron over the power-law electron distribution, Wijers & Galama (1999) find that $\psi(5.2) = 0.34$, therefore

$$\epsilon_{p,sy} = 3.2 \times 10^{-9} \gamma_p^2 B \Gamma \text{ eV} . \quad (19)$$

Using equation (16) and the observed $\epsilon_{p,sy}$, this leads to

$$B\Gamma = 4.9 \times 10^5 x_1^2 \text{ G} . \quad (20)$$

The received flux at the peak of the synchrotron spectrum is

$$F_{p, sy} = \frac{z+1}{4\pi D_L^2(z)} \Gamma L'_{p, sy} \quad (21)$$

where $D_L(z)$ is the burst luminosity distance, the factor Γ accounts for relativistic beaming of the burst emission (over the region $\theta < \Gamma^{-1}$, the specific flux is beamed by a factor Γ^3 , but that region has an area which is a fraction Γ^{-2} of the entire emitting surface, assuming spherical symmetry) and

$$L'_{p, sy} = \sqrt{3}\phi(p) \frac{e^3}{m_e c^2} B N \quad (22)$$

is the comoving-frame luminosity at $\epsilon'_{p, sy}$ and N is the number of radiating electrons (for a spherically symmetric outflow). The factor $\phi(p)$ calculated by Wijers & Galama (1999) is $\phi(5.2) = 0.70$.

The observed GRB and optical flux at any time may be the superposition of many (η) emission episodes (sub-pulses resulting from e.g. internal collisions in the outflow) in which a smaller number (N_e) of electrons radiate: $N = \eta N_e$. The superposition of these sub-pulses leads to intrinsic fluctuations in the burst light-curve, of relative amplitude $\eta^{-1/2}$. If the observing time resolution were shorter than the sub-pulse duration then the amplitude of the GRB light-curve fluctuations (which includes Poisson noise in addition to the source fluctuations) would represent an upper limit for the amplitude of the intrinsic source fluctuations. In that case, the less than 10% fluctuations of GRB 990123 displayed in figure 1 of Briggs et al. (1999) indicate that $\eta \gtrsim 100$. However, the sub-pulse duration which we obtain below, of about $\delta t = 20$ ms, is a factor 10 less than the typical $t_{res} = 256$ ms resolution of BATSE light-curves. In this case, there would be $N_{sp} = \eta(t_{res}/\delta t) \simeq 10\eta$ sub-pulses in a GRB pulse. The resulting amplitude of source fluctuations, $N_{sp}^{-1/2}$, is upper bound by the observed $\lesssim 10\%$ fluctuations of GRB 990123, hence $\eta \gtrsim 10$ suffices to accommodate the observed fluctuations. Normalizing η to 10, the synchrotron peak flux is

$$F_{p, sy} = 2.5 \times 10^{-53} \eta_1 B \Gamma N_e \text{ mJy} . \quad (23)$$

The observed synchrotron peak flux $F_{p, sy}$ and $B\Gamma$ from equation (20) lead to

$$N_e = 5.4 \times 10^{50} x_1^{-5/3} \eta_1^{-1} . \quad (24)$$

Because the synchrotron and inverse-Compton spectra are similar, the ratio Y of the inverse-Compton and synchrotron radiating powers is

$$Y = \frac{\epsilon_{p, ic} F_{p, ic}}{\epsilon_{p, sy} F_{p, sy}} = 2.4 x_1^{-4/3} = 0.82 \gamma_p^2 \frac{F_{p, ic}}{F_{p, sy}} \quad (25)$$

using equation (15). At the same time, the Compton parameter is the integral over the electron distribution of the average increase in the photon energy through scattering:

$$Y = \int_{\gamma_p}^{\infty} \frac{4}{3} \gamma^2 \frac{d\tau_e}{d\gamma} d\gamma = \frac{4}{3} \frac{p-1}{p-3} \gamma_p^2 \tau_e = 2.54 \gamma_p^2 \tau_e \quad (26)$$

where τ_e is the sub-pulse optical thickness to electron scattering and $d\tau_e/d\gamma \propto dN/d\gamma \propto \gamma^{-p}$. The above two equations lead to

$$\tau_e = 0.32 \frac{F_{p, ic}}{F_{p, sy}} = 7.1 \times 10^{-5} x_1^{-1/3} \quad (27)$$

using the synchrotron and peak fluxes of GRB 990123. The electron optical thickness is set by the electron column density:

$$\tau_e = \frac{\sigma_T}{4\pi} \frac{N_e}{r^2} \quad (28)$$

where σ_T is the Thomson cross-section. The last two equations allow the determination of the radius at which the burst and prompt optical emissions are released:

$$r_\gamma = 6.3 \times 10^{14} x_1^{-2/3} \eta_1^{-1/2} \text{ cm} . \quad (29)$$

The last observational constraint to be used is equation (5). The radiative cooling timescale of the γ_p -electrons is

$$t_c(\gamma_p) = \frac{z+1}{\Gamma} t'_c(\gamma_p) = 6\pi(z+1) \frac{m_e c}{\sigma_T} \frac{1}{\gamma_p B^2 \Gamma(Y+1)} \quad (30)$$

where $t'_c(\gamma_p)$ is the comoving-frame cooling timescale. Substituting B from equation (20) and Y from equation (25), leads to

$$t_c(\gamma_p) = 3.1 \times 10^{-5} x_1^{-13/6} \Gamma \text{ s} . \quad (31)$$

Because $t_c \propto \gamma^{-1}$, the cooling timescale for the γ_c -electrons, $t_c(\gamma_c)$, is a factor $\gamma_c/\gamma_p > 2.6$ smaller than the above $t_c(\gamma_p)$.

The lack of the signature of electron cooling in the spectrum of GRB 990123 means that the time t_Δ that the electrons spend radiating is smaller than $t_c(\gamma_c)$. The t_Δ represents the lifetime of the magnetic field in the shocked fluid. An estimate of it is provided by the time it takes the shocks to propagate through the shells that generate the burst emission. Shell spreading* is expected to yield a comoving-frame shell-thickness $\Delta' \sim r/\Gamma$, which is crossed by a relativistic shock in an observer-frame time

$$t_\Delta = (z+1) \frac{\Delta'}{c\Gamma} = 5.7 \times 10^4 x_1^{-2/3} \eta_1^{-1/2} \Gamma^{-2} \text{ s} \quad (32)$$

for a shell at the GRB radius r_γ given equation (29). Then, the condition $t_c(\gamma_c) > t_\Delta$ leads to a lower limit on the Lorentz factor of the shocked fluid:

$$\Gamma \geq 1660 x_1^{1/2} \eta_1^{-1/6} . \quad (33)$$

Substituting in equation (20), we find a lower limit on the magnetic field

$$B \leq 290 x_1^{3/2} \eta_1^{1/6} \text{ G} \quad (34)$$

while equation (32) yields an upper limit on the sub-pulse duration:

$$\delta t \leq 20 x_1^{-5/3} \eta_1^{-1/6} \text{ ms} . \quad (35)$$

Note that r , Γ , B and δt have a weak dependence on the somewhat uncertain number η of overlapping sub-pulses within a GRB pulse. and that the timescale for the source intrinsic fluctuations, δt , is smaller than the temporal resolution (256 ms) of GRB 990123 light-curve shown in figure 1 of Briggs et al. (1999), i.e. the source intrinsic fluctuations are averaged over 10 times the fluctuation timescale.

The comoving-frame peak-energy of the inverse-Compton spectrum is $\epsilon'_{p, ic} = (z+1)\epsilon_{p, ic}/\Gamma \lesssim 7 \times 10^{-4} m_e c^2$, hence $\gamma_p \epsilon'_{p, ic} \lesssim 0.07 m_e c^2$. This means that the second inverse-Compton scattering occurs around the

* The origin of the burst emission from a shell with this thickness is the only non-trivial assumption made in this section

Klein-Nishina reduction in the scattering cross-section. Integrating the Compton parameter given in equation (26) over the burst spectrum and electron distribution, and using the Klein-Nishina scattering cross-section, we obtain that the Compton parameter for the second scattering is $\tilde{Y} \gtrsim 0.89 \gamma_p^2 \tau_e = 0.82 x_1^{-4/3}$, i.e. a factor $\lesssim 3$ lower than Y for the first scattering. Therefore, the synchrotron self-Compton model implies the existence of a high-energy component, whose F_ν spectrum peaks at $\gamma_p^2 \epsilon_{e,ic} \sim 2 x_1^{-1}$ GeV and having a fluence $\Phi_{GeV} = \tilde{Y} \Phi_\gamma \gtrsim 3 \times 10^{-4}$ erg cm $^{-2}$.

4 IMPLICATIONS OF SYNCHROTRON SELF-COMPTON MODEL FOR GRB 990123

4.1 Jet edge

If the optical counterpart of GRB 990123 is indeed the large-angle emission produced during the second GRB pulse (i.e. if there is little contribution to the ROTSE optical emission from subsequent GRB pulses) then the optical light-curve should exhibit a sharp break when photons emitted from the edge of the jet ($\theta = \theta_{jet}$) arrive at the observer. From equation (6), this break should be seen at

$$t_{edge} = (z+1) \frac{r \theta_{jet}^2}{2c}, \quad (36)$$

which depends on the yet-undetermined jet opening.

The forward-shock optical emission of the afterglow 990123 exhibits a steepening at $t_{jet} \lesssim 3$ d (Figure 2). If attributed to a collimated outflow (Kulkarni et al. 1999), then the jet opening is

$$\theta_{jet} = \frac{1}{\tilde{\Gamma}(t_{jet})} \quad (37)$$

where $\tilde{\Gamma}$ is the Lorentz factor of the circumburst medium swept-up by the forward-shock, which can be calculated from the isotropic-equivalent kinetic energy E of the shock and the density of the circumburst medium:

$$E = 4\pi r A m_p c^2 \tilde{\Gamma}^2. \quad (38)$$

The above equation applies for a circumburst medium with a radial proton density distribution $n(r) = Ar^{-2}$, characteristic for the wind ejected by a massive star as the GRB progenitor, and results from that the comoving-frame energy-per-particle in the shocked medium is $\tilde{\Gamma}$. For the above the dynamics of the shocked medium, $\tilde{\Gamma} \propto r^{-1/2}$, integration of the equation for photon arrival

$$t = \frac{3(z+1)}{2c} \int^r \frac{dr'}{\tilde{\Gamma}^2(r')} \quad (39)$$

where the factor 3 relates $\tilde{\Gamma}$ to the arrival time of photons emitted from $\theta = \tilde{\Gamma}^{-1}$ (as most of the afterglow emission arises from this location), leads to

$$\tilde{\Gamma}(t) = \left(\frac{3E}{16\pi c A m_p c^2} \right)^{1/4} \left(\frac{t}{z+1} \right)^{-1/4}. \quad (40)$$

Taking the GRB output $E_\gamma = 3 \times 10^{54}$ ergs as an estimation of the forward-shock kinetic energy and parameterizing the wind medium density to that of a massive star ejecting $10^{-5} M_\odot \text{ yr}^{-1}$ at 10^3 km s^{-1} , i.e. $A = 3 \times 10^{35} A_* \text{ cm}^{-1}$, we obtain

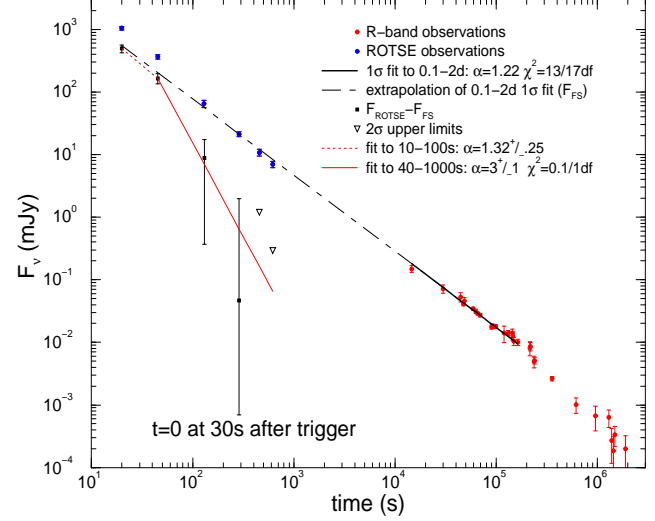


Figure 4. Same as in Figure 2, but using a steeper fit, $F_{FS} \propto t^{-1.23}$ instead of $F_{FS} \propto t^{-1.23}$. The ROTSE light-curve with the forward-shock emission subtracted exhibits now a sharp decline at $t \gtrsim 50$ s.

$$\tilde{\Gamma}(t_d) = 25 E_{54.5}^{-1/4} A_*^{-1/4} t_d^{-1/4} \quad (41)$$

where t_d is observer time measured in days.

From equations (37) and (41), the jet opening corresponding to a light-curve break at $t_{jet} \lesssim 3$ d is

$$\theta_{jet} \lesssim 0.052 E_{54.5}^{-1/4} A_*^{1/4} \text{ rad}. \quad (42)$$

Then, from equation (36) and (29), the large-angle emission should end at

$$t_{edge} \lesssim 74 x_1^{-2/3} \eta_1^{-1/2} E_{54.5}^{-1/2} A_*^{1/2} \text{ s}. \quad (43)$$

Coincidentally, this is about the same as the time $t_+ = x t_p = 80 x_1$ s when the peak energy of the synchrotron spectrum crosses the optical, i.e. there are two independent factors which imply the existence of a steeper decay of the large-angle emission after 80 s from the beginning of the second GRB pulse (110 s after trigger). This conclusion is at odds with the ROTSE light-curve shown in Figure 2 but is consistent with the optical counterpart emission after subtracting a slightly more steeply-decaying forward-shock contribution, as illustrated in Figure 4. The power-law fit to the 0.1–2 day optical light-curve shown in Figure 4 is statistically acceptable ($\chi^2 = 13/17$ dof) and has a decay index α larger than that of the best-fit shown in Figure 2 by 1σ .

4.2 Self-absorption photon energy

For the power-law electron distribution given in equation (4), the self-absorption linear coefficient at frequency ν is

$$\alpha_\nu = \frac{p+2}{8\pi} \frac{n_e}{(\gamma_p m_e c)^2} \nu^{-2} \int_{\gamma_p}^{\infty} d\gamma P_\nu(\gamma) \left(\frac{\gamma}{\gamma_p} \right)^{-(p+1)} \quad (44)$$

where n_e is the electron density and

$$P_\nu(\gamma) = \frac{\sqrt{3}\pi}{4} \frac{e^3 B}{m_e c^2} F\left(\frac{\nu}{\nu_c}\right), \quad \nu_c = \frac{3}{16} \frac{e}{m_e c} B \gamma^2 \quad (45)$$

is the synchrotron specific emissivity per electron, $F(x) = x \int_x^\infty K_{5/3}(\xi) d\xi$ being the synchrotron function ($K_{5/3}$ is

the modified Bessel function of index 5/3) and ν_c the synchrotron characteristic frequency for electrons of energy $\gamma m_e c^2$.

At $\nu \ll \nu_c(\gamma_p)$, the synchrotron function is

$$F(y) \simeq 2.15 y^{1/3} \quad (46)$$

and the integral in equation (44) can be calculated analytically, leading to the following optical thickness to synchrotron self-absorption, $\tau_a(\nu) = (\alpha_\nu \tau_e)/(n_e \sigma_T)$,

$$\tau_a(\nu) = 3.3 \frac{p+2}{p+2/3} \frac{e \tau_e}{\sigma_T B \gamma_p^5} \left[\frac{\nu}{\nu_c(\gamma_p)} \right]^{-5/3}. \quad (47)$$

For $p = 2.5$ and the parameters B , τ_e and γ_p derived in the section §3, the synchrotron optical thickness at photon energy ϵ is

$$\tau_a(\epsilon) \gtrsim 5.1 \times 10^{-2} x_1^{2/3} \eta_1^{-1/6} \left(\frac{\epsilon}{\epsilon_{p, sy}} \right)^{-5/3}. \quad (48)$$

Therefore, the self-absorption energy of the synchrotron spectrum, defined by $\tau_a(\epsilon_{a, sy}) = 1$, is

$$\epsilon_{a, sy} \gtrsim 0.17 x_1^{2/5} \eta_1^{-1/10} \epsilon_{p, sy} = 3.3 x_1^{7/5} \eta_1^{-1/10} \text{ eV}. \quad (49)$$

If $\epsilon_{a, sy}$ were above the optical, then $\beta_o = 2$ and the large-angle emission would be flat (from equation 1). That the ROTSE optical light-curve decays, implies that $\epsilon_{a, sy}$ is below the optical domain. Then equation (49) leads to

$$x \lesssim 10 \eta_1^{1/14}. \quad (50)$$

which is close to the upper limit obtained by requiring that the synchrotron flux does not overshine the inverse-Compton emission at 2 keV (equation 14). The synchrotron self-absorption energy given in equation (49) implies that the up-scattered self-absorption energy is

$$\epsilon_{a, ic} \gtrsim \frac{4}{3} \gamma_p^2 \epsilon_{a, sy} = 57 x_1^{2/5} \eta_1^{-1/10} \text{ keV}, \quad (51)$$

where the $(4/3) \gamma_p^2$ factor is the average increase of the up-scattered photon energy.

BeppoSAX observations of GRB 990123 (Corsi et al. 2006) have shown that, at the epoch of the first two ROTSE measurements shown in Figure 2, the burst $F_\nu \propto \nu^{1/3}$ spectrum extends down to 2 keV, i.e. a for an other 1.5 dex in energy below the $\epsilon_{a, ic}$ obtained in equation (51). The up-scattered spectrum below $\epsilon_{a, ic}$ is $F_\nu \propto \nu$ (and not $\propto \nu^2$, as for the synchrotron spectrum below $\epsilon_{a, sy}$), thus the synchrotron self-Compton model flux at 2 keV flux would be a factor ~ 30 below that observed by BeppoSAX. A reduction by a factor 2 of that factor is obtained by integrating the up-scattered radiation over the synchrotron and electron distribution which, as shown in Figure 3. We conclude that, for $\epsilon_{a, ic} \gtrsim 57$ keV, the numerically calculated synchrotron self-Compton model flux at 2 keV is a factor $\gtrsim 10$ below that without self-absorption (i.e. below the BeppoSAX flux) and that a reduction of $\epsilon_{a, ic}$ by a factor larger than 10 is required to bring the synchrotron self-Compton model in accord with observations.

4.3 Decaying magnetic field

The above difficulty encountered by the synchrotron self-Compton model and the large-angle emission interpretation

of the ROTSE counterpart, i.e. the high up-scattered self-absorption energy, is alleviated if the magnetic field does not fill the entire shocked region (of radial length Δ'), but decays to a negligible value at some distance $b\Delta'$ ($b < 1$) behind the shock which energize the emitting fluid. This implies a reduction of the synchrotron flux $F_{p, sy}$ (equation 23) by a factor b , which must be compensated by increasing the number of electrons N_e (equation 24) by a factor b^{-1} , as the product $B\Gamma$ is fixed by the peak-energy of the synchrotron spectrum (equation 20). The Compton parameter Y and the minimum electron Lorentz factor γ_p remain the same, because they are the γ -ray-to-optical fluences ratio (equation 25) and the square-root of the γ -ray-to-optical peak-energies ratio (equation 16), respectively, hence the optical thickness τ_e of all electrons (within and outside the region filled with magnetic field) is unchanged.

Consequently, the emission radius $r \propto (N_e/\tau_e)^{1/2}$ (equation 28) increases by a factor $b^{-1/2}$. This means that the time $t_{edge} \propto r$ when the jet edge is seen (equation 36) increases by the same factor $b^{-1/2}$ and that large-angle emission can last longer than given in equation (43).

As for self-absorption, a decaying magnetic field means that the column density of the electrons embedded in the magnetic field (i.e. the electrons which absorb the synchrotron flux) is a fraction b of the total electron column density, hence τ_a of equation (47) is multiplied b and the up-scattered self-absorption energy $\epsilon_{a, ic} \propto \tau_a^{3/5}$ by $b^{3/5}$. The dependence of τ_e on the filling factor b is slightly different if the Lorentz factor is at the lower limit implied by the condition $\gamma_c \gtrsim 2.6 \gamma_p$ (which lead to equation 33) and the magnetic field at the upper limit corresponding to equation (20). If the electron radiative cooling is synchrotron dominated ($Y < 1$) then the time electrons spend in the magnetic field and cool becomes bt_Δ (equation 32) while, if scatterings dominate ($Y > 1$), the electron cooling timescale (equation 31) becomes $t_c(\gamma_p)/b$ because the intensity of the synchrotron emission to be up-scattered is b times lower. Thus, in either case, the condition $\gamma_c \gtrsim 2.6 \gamma_p$ for electron cooling during the burst leads to $t_c(\gamma_p) > 2.6 bt_\Delta$, consequently the lower limit on the Lorentz factor Γ (equation 33) decreases by a factor $b^{-1/6}$ and the upper limit on B resulting from equation (20) increases by a factor $b^{-1/6}$. It follows that, if the magnetic field strength B is at its upper limit, $\epsilon_{a, ic}$ of equation (51) gets multiplied by a factor $b^{7/10}$, which is close to the $b^{3/5}$ factor inferred above for the case when Γ above its lower limit.

Thus, for

$$b \lesssim 0.05 x_1^{-4/7} \eta_2^{1/7} \quad (52)$$

the up-scattered self-absorption energy is lowered by a factor 10 and the model flux at 2 keV becomes compatible with BeppoSAX observations of GRB 990123. Parameterizing $b = 0.03 b_{-1.5}$, we find that the GRB emission is produced at

$$r_\gamma = 1.2 \times 10^{15} x_1^{-2/3} \eta_2^{-1/2} b_{-1.5}^{-1/2} \text{ cm} \quad (53)$$

the lower limit on the outflow Lorentz factor is

$$\Gamma \geq 630 x_1^{1/2} \eta_2^{-1/6} b_{-1.5}^{1/6} \quad (54)$$

and the upper limit on the magnetic field is

$$B \leq 760 x_1^{3/2} \eta_2^{1/6} b_{-1.5}^{-1/6} \text{ G}. \quad (55)$$

The sub-pulse duration of equation (32) is now $t_\Delta \leq 0.25 x_1^{-5/3} \eta_2^{-1/6} b_{-1.5}^{-5/6}$ s, therefore the source intrinsic fluctuations are marginally resolved and the observed fluctuation amplitude of about 10% requires that $\eta \simeq 100$, which is the canonical value chosen in the above equations. Requiring that the sub-pulse duration t_Δ does not exceed the FWHM duration of a GRB pulse, which is $t_\gamma \simeq 10$ s, leads to

$$b > 6 \times 10^{-4} x_1^{-2} \eta^{-1/5} \quad (56)$$

with $\eta \gtrsim 1$ because, for $t_\Delta \simeq t_\gamma$, the GRB pulse should be a single emission episode.

The comoving-frame electron density of the shocked fluid is

$$n' = \frac{N_e}{4\pi r^2 (\Delta'/\zeta)} \geq 5.8 \times 10^7 \zeta x_1^{5/6} \eta_2^{1/3} b_{-1.5}^{2/3} \text{ cm}^{-3} \quad (57)$$

where ζ is the shock compression factor. Therefore, the magnetic field energy is a fraction

$$\varepsilon_B = \frac{B^2/8\pi}{\Gamma' n' m_p c^2} \simeq 0.27 x_1^{13/6} (\Gamma' - 1)^{-1} \zeta^{-1} b_{-1.5}^{-1} \quad (58)$$

of the energy density in the shocked fluid, where Γ' is the Lorentz factor of the shock energizing the GRB-emitting fluid measured in the frame of the yet unshocked plasma. If the GRB ejecta were not initially highly magnetized then a sub-equipartition magnetic field ($\varepsilon_B < 0.5$) requires that $b > 0.03 x_1^{13/6} (\Gamma' - 1)^{-1} \zeta^{-1}$. For a relativistic shock with $\Gamma' \sim \text{few}$ and $\zeta = 4\Gamma'$, this condition becomes

$$b \gtrsim 10^{-4} x_1^{13/6} \quad (59)$$

which is close to that obtained by requiring that $t_\Delta \lesssim 10$ s (equation 56).

Thus, we find that the magnetic field length-scale is a fraction $b = 10^{-3.5} - 10^{-1.5}$ of the thickness of the shocked gas. For the comoving-frame density given in equation (57), the plasma skin-depth in the shocked gas is

$$\lambda = c \left(\frac{\pi \gamma_p m_e}{e^2 n'} \right)^{1/2} \geq 1.1 \times 10^3 x_1^{-2/3} \eta_2^{-1/6} b_{-1.5}^{-1/3} \text{ cm} \quad (60)$$

thus the magnetic field decay length-scale, $b(\Delta'/\zeta)$, is $5 \times 10^5 - 10^7$ times larger than the plasma skin-depth.

Lastly, we note that radius at which the expansion of the ejecta is affected by the interaction with the circumburst medium, obtained by using the GRB ejecta Lorentz factor Γ instead of the Lorentz factor of the shocked medium, $\tilde{\Gamma}$, in equation (38), is

$$r_{dec} \lesssim 1.4 \times 10^{15} E_{54.5} A_*^{-1} x_1^{-1} \eta_2^{1/3} b_{-1.5}^{-1/3} \text{ cm} \quad (61)$$

which is close to the radius r_γ where the burst emission is produced (equation 53). This shows that, if the burst mechanism were internal shocks in a variable wind, the dynamics of these internal shocks is affected by the deceleration of the outflow and, perhaps, a large number of collisions are between ejecta shells and the decelerating leading edge of the outflow. That the deceleration radius is comparable with the prompt emission radius is consistent with the subtraction of the back-extrapolated forward-shock emission from the optical prompt flux done for Figures 2 and 4: in the $r_{dec} > r_\gamma$ case, the power-law decay of the forward-shock emission would set in only after r_{dec} and the 0.1–2 day optical decay could be extrapolated backwards only up to an epoch which is after the burst.

5 CONCLUSIONS

The underlying assumption of this work, that the ROTSE optical counterpart of GRB 990123 arose from the same mechanism as the burst, is motivated by the similarity of its timing and decay rate to those of the fast-decay phase of Swift X-ray afterglows. As the latter can be identified with the large-angle emission produced during the burst, we attribute the ROTSE optical counterpart to the same mechanism. However, the optical emission associated with GRB 990123 must be a different spectral component than the burst because the optical flux lies well above the extrapolation of the burst spectrum. In this way, we arrived at the synchrotron self-Compton model for GRB 990123 and its optical counterpart.

The spectral slope of the optical counterpart of GRB 990123 was not measured. Future observations of early optical afterglows will provide a very simple test of the large-angle emission for GRB optical counterparts: their power-law decay index and spectral slope should satisfy equation (1). The synchrotron self-Compton interpretation of the optical and γ -ray emissions of GRB 990123 implies that the optical spectral slope must be equal to either the low-energy or the high-energy burst spectral slope. The decay index of the optical emission of GRB 990123 and the slope of the burst continuum below its peak satisfy equation (1), thus providing support to the large-angle interpretation proposed for the optical counterpart.

In the framework of the synchrotron self-Compton model, the ROTSE optical and BATSE γ -ray observations for GRB 990123 allow us to determine that the radius at which the burst emission was produced is comparable to the outflow deceleration radius, which in itself does not rule out any of the possible origins (internal, reverse-external, or forward-external shocks) of the burst emission, but points to that, if the burst arises from internal shocks, then most of these shocks must have occurred on the decelerating, leading front of the outflow, as proposed by Fenimore & Ramirez-Ruiz (1999). Alternatively, that the burst emission was produced at the deceleration radius gives support to the electromagnetic model of Lyutikov & Blandford (2003), which predicted such a burst location.

The outflow parameters derived from the optical and γ -ray properties of GRB 990123 imply an up-scattered self-absorption frequency of 60 keV, which is inconsistent with BeppoSAX observations, showing an optically-thin burst spectrum above 2 keV. This difficulty can be overcome if the magnetic field does not occupy the entire shocked gas. The magnetic field decay length-scale is upper-bound by the condition that the burst spectrum is optically thin above 2 keV and lower-bound by that the shell shock-crossing time should not be longer than the duration of a GRB pulse and the magnetic field energy should not exceed equipartition. From these conditions, we find that the magnetic field must occupy $10^{-3} - 10^{-2}$ of the shocked shell, which is equal to $10^6 - 10^7$ plasma skin-depths. It is rather puzzling that the magnetic field decay-length is so much larger than the natural scale for magnetic field generation, and yet does not occupy the entire shell of shocked gas. Whether such a large magnetic field decay length-scale is possible remains an open question which cannot be currently addressed by numerical models of two-stream instabilities (Medvedev & Loeb 1999),

due to the large computational effort required to follow the evolution of magnetic fields over such long scales. We note that other researchers have obtained similar constraints on the magnetic field decay length-scale: from energetic arguments related to the outflow parameters obtained through afterglow modelling, Rossi & Rees (2003) have set a low limit of 10^{-2} on the fraction of shell filled by magnetic field, while Pe'er & Zhang (2006) have inferred a decay length-scale smaller by a factor 10 than our value, from the condition that, in internal-shocks synchrotron-emission GRBs, electrons do not cool significantly during the burst.

There are two other bursts whose accompanying optical emission has been measured. The optical and γ -ray light-curves of GRB 041219A (Vestrand et al. 2005) are correlated and the post-burst decay of the optical counterpart exhibits variability (Blake et al. 2005), both indicating that the counterpart is not the large-angle emission released during the burst. The optical and γ -ray emissions of GRB 050820A (Vestrand et al. 2006, Cenko et al. 2006) are not correlated, consistent with the large-angle emission scenario, but the t^{-1} post-burst decay of the optical afterglow is too slow for that interpretation: the burst spectrum, $F_\nu \propto \nu^{-0.1 \pm 0.1}$, and equation (1) imply a steeper, t^{-2} decay for the large-angle emission. Therefore, GRB 990123 is so far the only case exhibiting a fast-decaying optical counterpart, uncorrelated with the burst emission, that can be interpreted as arising from the same mechanism as the burst.

REFERENCES

- Akerlof C. et al. , 1999, *Nature*, 398, 400
 Blake C. et al. , 2005, *Nature*, 435, 181
 Blumenthal G. & Gould R., 1970, *Rev. of Modern Phys.*, 42, 237
 Briggs M. et al. , 1999, *ApJ*, 524, 82
 Cenko B. et al. , 2006, *ApJ*, accepted (astro-ph/0608183)
 Corsi A. et al. , 2006, *A&A*, 438, 829
 Fan Y., Dai Z., Huang Y., Lu T., 2002, *Chin. J. A&A*, 2, 449
 Fenimore E. & Ramirez-Ruiz E., 1999 (astro-ph/9909299)
 Galama T. et al. , 1999, *Nature*, 398, 394
 Kobayashi S. & Sari R., 2000, *ApJ*, 542, 819
 Kulkarni S. et al. , 1999, *Nature*, 398, 389
 Kumar P. & Panaitescu A., 2000, *ApJ*, 541, L51
 Kumar P. et al. , 2006, *MNRAS*, 367, L52
 Lyutikov M. & Blandford R., 2003, *Bull. of AAS*, vol 35, p 622
 McMahon E., Kumar P., Piran T., 2006, *MNRAS*, 366, 575
 Medvedev M. & Loeb A., 1999, *ApJ*, 526, 697
 Mészáros P. & Rees M., 1999, *MNRAS*, 306, L39
 Nakar E. & Piran T., 2005, *ApJ*, 619, L147
 Nousek J. et al. , 2006, *ApJ*, 642, 389
 O'Brien P. et al. , 2006, *ApJ*, 647, 1213
 Panaitescu A. & Mészáros P., 1998, *ApJ*, 492, 683
 Panaitescu A. & Mészáros P., 2000, *ApJ*, 544, L17
 Panaitescu A. & Kumar P., 2004, *MNRAS*, 353, 511
 Panaitescu A. et al. , 2006, *MNRAS*, 369, 2059
 Pe'er A. & Zhang B., 2006, *ApJ*, accepted (astro-ph/0605641)
 Preece R. et al. , 1998, *ApJ*, 506, L23
 Rossi E. & Rees M., 2003, *MNRAS*, 339, 881
 Sari R. & Piran T., 1999, *ApJ*, 517, L109
 Soderberg A. & Ramirez-Ruiz E., 2002, *MNRAS*, 330, L24
 Stern B. & Poutanen J., 2004, *MNRAS*, 352, L35
 Vestrand W. et al. , 2005, *Nature*, 435, 178
 Vestrand W. et al. , 2006, *Nature*, 442, 172
 Wijers R. & Galama T., 1999, *ApJ*, 523, 177
 Zhang B. et al. , 2006, *ApJ*, 642, 354